J. Hydrol. Hydromech., 71, 2023, 1, 11–21
https://doi.org/10.2478/johh-2022-0042


sciendo Journal of Hydrology and Hydromechanics Institute of Hydrology SAS

# Effects of pore size and pore connectivity on trapped gas saturation

Caroline H. Dias[1*], Felipe M. Eler[1], Carlos Cordeiro[1], Mateus G. Ramirez[1], José A. Soares[2], Denise Nunes[1], Maira C.O. Lima[1], Paulo Couto[1]

[1] Department of Civil Engineering, COPPE, Federal University of Rio de Janeiro, RJ, Brazil.
[2] Department of Mining Engineering, Federal University of Campina Grande, Paraíba, PB, Brazil.
[*] Corresponding author. E-mail: caroldias@petroleo.ufrj.br

**Abstract:** Trapped or residual air (or gas) is known to affect the multiphase hydraulic properties of both soils and rocks. Trapped air is known to impact many vadose zone hydrologic applications such as infiltration and flow in the capillary fringe, but is also a major issue affecting recoverable oil reserves. Although many studies have focused on the relationship between porosity and trapped gas saturation ($S_{gt}$) in sandstones, far fewer studies have been carried out for carbonate rocks. This work aims to analyze the influence of porous media properties on trapped gas saturation in carbonate rocks. For this we used thirteen Indiana Limestone and Silurian dolomite rock samples from the USA, and several coquinas from the Morro do Chaves formation in Brazil. Pore size distributions were obtained for all samples using Nuclear Magnetic Resonance (NMR), and Mercury Injection Capillary Pressure (MICP) data from three of the samples to determine their pore throat size distributions. Additionally, 3D microtomography (microCT) images were used to quantify macropore profiles and pore connectivities. Results indicate a lower capacity of gas trapping in carbonate rocks in which micro- and mesopores predominate. Results also indicate that in carbonate rocks, pore size exerts a greater influence on the ability of gas trapping compared to pore connectivity, so that rocks with a predominance of macropores have greater capacity for gas trapping, even when the macropores are well interconnected. These findings show that pore characteristics very much affect the processes governing gas trapping in carbonate rocks, and indirectly the multiphase hydraulic properties and recoverable oil reserves of carbonate rock reservoirs.

**Keywords:** Trapped gas; Carbonate rocks; Pore size distribution; Coordination number.

## INTRODUCTION

Air or gas trapping in porous media occurs during displacement of an initially present non-wetting phase by an infiltrating wetting phase (Mohammadian et al., 2015; Raeini et al., 2015; Tanino and Blunt, 2012). Trapped air can significantly affect multiphase flow phenomena in vadose zone hydrologic applications such as infiltration and flow processes in the capillary fringe (e.g., Faybishenko, 1995; Fayer and Hillel, 1986; Gonçalves et al., 2019; and references therein). Gas trapping plays an important role also in hydrocarbon recovery and carbon capture and storage (CCS) processes (Fatemi and Sohrabi, 2013; Wang et al., 2016). Regarding hydrocarbon recovery efficiency, capillary trapping of gas reduces residual oil saturation (Afzali et al., 2018; Element et al., 2003). In case of CCS, the main objective is to maximize capillary trapping to increase $CO_2$ storage (e.g., Ruspini et al., 2017). These various studies show that air or gas trapping is a function of many parameters, including the prevailing wetting rate, wettability, and especially grain texture and pore structure.

Understanding and quantifying the effects of trapped gas in oil reservoirs is a challenge, particularly for carbonate rocks which have an unusually complex multiscale heterogeneous pore structure causing unique fluid retention and flow properties (Godoy et al., 2019; Sun et al., 2017). Carbonate hydrocarbon reservoirs, including the Brazilian Pre-Salt, are the subject of several scientific investigations due to their geological complexity and economic value (Herlinger et al., 2017; Lima et al., 2022).

One of the main uncertainties in estimating recoverable reserves of oil fields is the large variation in observed values of trapped gas saturation ($S_{gt}$). Various experimental and simulation studies have been conducted to assess how selected porous media properties affect the degree of gas trapping (e.g., Bona et al., 2014; Jerauld, 1997). Pore structure and pore connectivity play especially a key role in the gas trapping process. Gas trapping is favored when wide pores are connected to narrow throats, with a well-connected pore system disfavoring gas trapping (Krevor et al., 2015). Fatemi and Sohrabi (2013) verified the influence of wettability on gas trapping. They observed that wettability to water leads to more gas trapping, probably due to increased snap-off in such systems. Suzanne et al. (2003), Tanino and Blunt (2013), and Kazemi et al. (2020), among others, found that trapped gas saturation ($S_{gt}$) tended to increase with initial gas saturation ($S_{gi}$). Various studies have looked at the specific relationships between porosity ($\emptyset$) and trapped gas saturation ($S_{gt}$), including factors causing values to deviate from established correlations. Most of these studies involved sandstone rocks. For example, Hamon et al. (2001) performed 300 $S_{gt}$ measurements on samples taken from three different sandstone gas reservoirs to analyze their variation and trend with petrophysical properties. $S_{gt}$ values ranged from 5% to 85%, with the plot of $S_{gt}$ values versus porosity showing two trends. For porosity values below 14%, Fontainebleau samples showed an increase in $S_{gt}$ as the porosity decreased, while $S_{gt}$ values decreased for two sandstones. For samples with porosities above 14%, $S_{gt}$ values were on average 25–35% for the three analyzed reservoirs. In these samples, clay presence was detected, showing that the amount of clay controls the $S_{gt}$. The authors concluded that increasing the clay content decreased gas trapping. Suzanne and Billiote (2004) studied the influence of microporosity on $S_{gt}$ in sandstones samples. They found that microporosity did not retain gas due to the proportion between pore bodies and pore throat

sizes and the gas diffusion mechanism. Ni et al. (2019) correlated several trapping coefficients (notably the linear and nonlinear Land trapping coefficients) with a range of petrophysical parameters (porosity, permeability, heterogeneity degree) estimated using computer tomography (CT) images. They found that the trapping capacity of sandstones decreased with porosity and increased with the degree of heterogeneity of the samples, but that the pore size distribution had little or no impact on the degree of $CO_2$ trapping. Kazemi (2020) evaluated the effects of different parameters, including porosity, on $S_{gt}$ in unconsolidated sandstones samples. They also observed that increasing the porosity led to a decrease in $S_{gt}$, consistent with other studies. No favorable scenario was found for the snap-off trapping processes in regions of high porosity. Compared to sandstones, relatively few gas trapping studies have focused on carbonate rocks. Tanino and Blunt (2012) evaluated the effects of pore structure on capillary trapping in both sandstone and carbonate samples. They found that capillary trapping increased mostly with increasing pore body-to-throat aspect ratios and tended to decrease with higher pore coordination numbers. They also correlated trapped saturation with the microporosity fraction of the pore volume but could not find a consistent relationship between these two parameters. The microporosity part of their samples had a pore aspect ratio and connectivity similar as those of the macroporosity region. In another study, Khisamov et al. (2020) proposed a method for estimating the saturation of trapped gas based on quantitative characteristics of the pore space structure and wettability. They found that the ratio between pore bodies and pore throats controlled the trapping capacity of their carbonate samples. They also showed that carbonate rocks with large pores, especially when water-wet, had higher trapped gas saturations. Our preliminary research showed a decreasing trend of $S_{gt}$ values with increasing porosity, similarly as several earlier studies (e.g., Kazemi, 2020; Ruspini, 2017). However, we noted a significant variation in the $S_{gt}$ values for samples with similar porosity. This indicated that, in addition to porosity, other factors must have affected $S_{gt}$. Motivated by these initial results, we investigated the influence of specific properties on $S_{gt}$ of carbonate rocks samples. Nuclear magnetic resonance (NMR), capillary pressure by mercury injection (MICP) and 3D microtomography images (microCT) were used to obtain a better understanding of the complete pore space, including microporosity and pore connectivity.

## MATERIALS AND METHODS

In total, 46 carbonate rock samples were used for the $S_{gt}$ analyses. The samples had porosities between 6% and 29.6%, and permeability between 1.70 mD and 1440 mD. Of these samples, 13 were used to analyze the pore size distribution using NMR. The 13 samples were selected based on part of a $S_{gt}$ versus porosity plot which showed the greatest variability in the measured gas saturation values. Fig. 1 shows a graph of $S_{gt}$ versus porosity for all carbonate samples. At a porosity of about 15%, the values of $S_{gt}$ varied from 18.4% to 64.3%. The 13 samples at or near this porosity value we selected for analysis of the pore size distribution; they are highlighted in Fig. 1 with different colors and grouped in terms of Indiana limestones (IL), coquinas (MC) from the Morro do Chaves formation in Brazil (Silveira et al., 2022), and silurian dolomites (SD).

Table 1 provides a list of the carbonate samples that were used, along with standard petrophysical properties (porosity and permeability) of the samples and measured trapped gas values. Below we provide details about the various measurements.

### Trapped gas saturation tests

Procedures for estimating $S_{gt}$ followed closely the approach described by Aissaoui (1983). Samples (5.0 cm long and 3.8 cm in diameter) were kept first for 24 hours in a controlled humidity oven at (60 °C and a relative humidity of 40%) to ensure completely dry plugs with air saturations at near 100%. Coreflood tests were subsequently performed to determine air-water $S_{gt}$ values by imbibing water under laboratory conditions. We used a confining pressure of 1,000 psi (6.89 MPa) and ambient fluid pressures, with the temperature being 21 ºC.

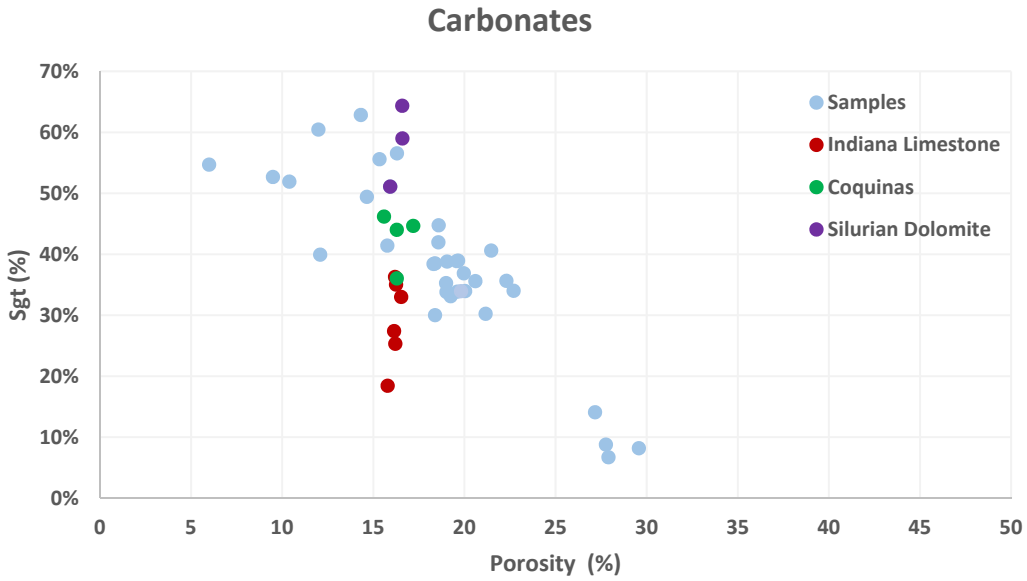


**Fig. 1.** Trapped gas saturation ($S_{gt}$) versus porosity for all carbonate samples. The samples selected for the pore size distribution analysis are highlighted according to their geological formation: Indiana Limestones (red circles), Coquinas (green circles), and Silurian Dolomites (purple circles).

**Table 1**. Measured porosities ($Ø$), permeabilities ($k$) and trapped gas saturations ($S_{gt}$) 13 carbonate rock samples.

| Samples | $Ø$ (%) | $k$ (mD) | $S_{gt}$ (%) |
|---|---|---|---|
| IL_09_01 | 16.3 | 10.9 | 35.0 |
| IL_09_02 | 16.5 | 18.7 | 33.0 |
| IL_09_03 | 16.1 | 10.5 | 27.4 |
| IL_09_04 | 16.2 | 14.0 | 25.3 |
| IL_09_05 | 15.8 | 7.4 | 18.4 |
| IL_09_06 | 16.2 | 15.5 | 36.3 |
| MC15P1_B | 16.3 | 10.6 | 36.0 |
| MC15P2 | 15.6 | 13.9 | 46.2 |
| MC20P1 | 16.3 | 208.6 | 44.0 |
| MC20P2 | 17.2 | 296.4 | 44.6 |
| SD_35_03 | 16.6 | 1338.9 | 64.3 |
| SD_35_04 | 16.6 | 1326.5 | 59.0 |
| SD_35_05 | 15.9 | 117.3 | 51.0 |

The experimental apparatus comprised a positive displacement pump, a confinement cell, pressure differential measurement transducers, graduated glassware, and an image capture system (Fig. 2).

After inserting the sample into the core holder, the confining pressure was raised to 1,000 psi (6.89 MPa, the same confining pressure used to measure the routine core properties). A positive displacement pump was used to inject distilled water into the system at a flow rate of 1 cm³/min. The distilled water was carefully deaired to ensure that no gas was injected into the sample and during the imbibition. The gas initially contained in the dry samples was displaced and collected at the equipment outlet during a period of 24 hours. This information was recorded, along with the time and temperature at which production occurred, to yield estimates of $S_{gt}$.

**Nuclear magnetic resonance (NMR)**

Nuclear Magnetic Resonance (NMR) is a technique that stands out in the investigation of the physical and chemical properties of materials in the oil and gas industry (Trevizan, et al., 2014). The transverse relaxation time $T_2$ is obtained through controlled radiofrequency pulses applied to previously saturated rock samples. From $T_2$ it is possible to obtain various information about the porous system, such as porosity, pore distribution, and permeability estimation, among others (Alyafei, 2015).

Before the tests, the samples were submitted to vacuum for 8 h, and subsequently saturated with 30,000 ppm of a KCl solution at a constant pressure of 1.500 psi (10.34 MPa) to minimize possible reactions of clay material in the samples.

To estimate the percentage of pores capable of retaining fluids by capillarity, the NMR analyzes were performed with the samples at complete saturation and after centrifugation, thereby providing estimates of irreducible saturation ($S_{wi}$) for determination of the $T_2$ cut-off value. The $T_2$ cut-off value is an essential parameter in NMR measurements since its value differentiates pores occupied by free fluid from pores occupied by fluid trapped by capillarity. This approach assumes that free fluids occupy large pores while irreducible fluid preferentially occupies the smaller pores (Lai et al., 2018).

The equipment used to acquire the NMR data was a low-field Oxford spectrometer (model Geospec+ 12/53 3D Imager). Following the methodology of Meiboom and Gill (1958), the CPMG sequence widely used in petrophysics was applied, leading to estimates of the porosity and pore size distribution. The approach assumes that decay (relaxation) during magnetization is proportional to the volume/surface ratio of a single pore/throat, which makes it possible to obtain the pore size ($r$) using

$$r = V/S = \rho_2 T_2 \quad (1)$$

where $V/S$ is the volume to surface ratio (μm), $\rho_2$ is the surface relaxivity (a rock specific scalar constant) (μm/ms), and $T_2$ is the transverse relaxation time.

**Mercury intrusion capillary pressure (MICP)**

Mercury intrusion capillary pressure (MICP) tests, in turn, are widely used to assess the complexity and heterogeneity of the pore throat structure (Li et al., 2016; Washburn, 1921). Through this test, the capillary pressure curve per pore volume is obtained, which can be transformed into a size distribution of the pore throat radii. For the MICP measurements we placed the rock samples is in a closed container under vacuum, and then filled the container with mercury. Initially, pressure is used to fill the largest pores, and as the pressure is increased, the mercury can enter the smaller pores, thereby allowing all pores at the end of the experiments to be filled with the non-wetting fluid (Washburn, 1921). The pore throat radii are then calculated from the pressure data using

$$P_c = \frac{2\sigma|\cos\theta|}{R_t} \quad (2)$$

where $P_c$ is the capillary pressure (MPa), $R_t$ is the throat radius (μm), $\sigma$ is the surface tension (mN/m) and $\theta$ is the contact angle (◦). Since MICP is a destructive technique, three subsampled plugs (SD_35_03, MC20P2, and IL_09_05) were selected to obtain the pore throat size distribution curves.

Integration of NMR and MICP results provides estimates of the surface relaxivity ($\rho_2$), which is needed to calibrate the relaxation time curve $T_2$ to produce the pore size distribution (Fleury and Romero-Sarmiento, 2016). Approximating the pore network

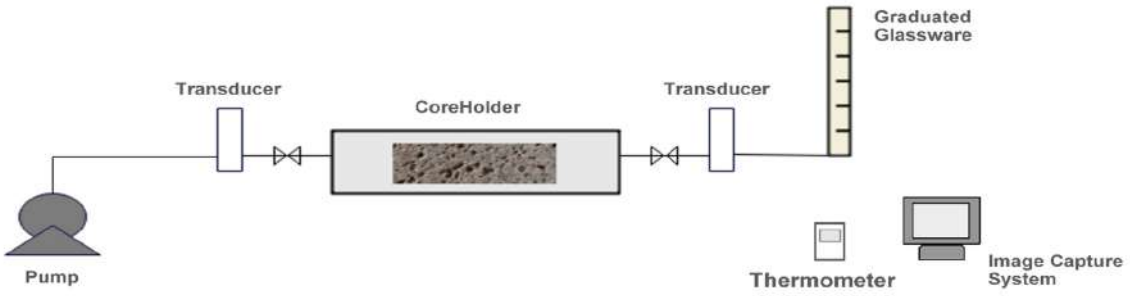


**Fig. 2.** Experimental setup used for the trapped gas ($S_{gt}$) measurements.

as a bundle of cylindrical capillary tubes of radius $r$, the pore structure can be correlated with $T_2$ by means of $\rho_2$ according to:

$$\left(\frac{S}{V}\right)_{cylinder} = \frac{2\pi rl}{\pi r^2 l} = \frac{2}{r} \rightarrow r_{spherical} = 3\rho_2 T_2 \quad (3)$$

where $l$ is the length of the capillary, and 3 a shape parameter for pores considered to be spherical (Ge et al., 2021; Lima et al., 2020). If the pores are considered cylindrical, the shape parameter becomes 2.

**X-ray microtomography (microCT)**

Investigations of pore structures at scales ranging from micrometers to a few millimeters are possible using microCT scanners that provide non-destructive 3D images of the internal structure of materials (Lima et al., 2022). Image acquisitions were performed using CoreTOM equipment (Tescan/XRE) with a 25 µm voxel size, while the images were reconstructed using the Acquila reconstruction software (Tescan/XRE). Image processing was carried out using Avizo 9.5 (Thermo Fisher Scientific). Image segmentation into pores and the mineral matrix (Fig. 3) was performed using the threshold tool (Otsuki et al., 2006). Threshold values were determined by comparing the pixel size with the NMR curve, with $T_2$ values first being converted to pore radii using Eq. (3) (Lima et al., 2020). After this, the pore structure was analyzed by transforming the pore space into a skeleton showing individual pores and throats in the pore network (Wildenschild and Sheppard, 2013). The skeleton was subsequently used in the PoreFlow software (Raoof et al., 2013) to obtain a more complete quantitative understanding of the entire pore system.

## RESULTS AND DISCUSSION

**Pore size distribution analysis using $T_2$ distribution graphs**

Porosity values obtained using NMR showed good agreement with the routine core measurements, and hence were considered to be of good quality. According to Souza (2012), the porosity values obtained by these two techniques are not expected to be the same, but they should have errors less than approximately about 2%.

The pore size distributions were analyzed using $T_2$ relaxation time distributions since the $T_2$ values are proportional to pore size, with its amplitude being directly related to the incremental porosity of the sample (Shao et al., 2017). Silva et al. (2015) partitioned the pores of carbonate rocks into five different families: micropores ($T_2$ values up to 1 ms), a transition from micropores to mesopores (1 to 10 ms), mesopores (10 to 100 ms), a transition from mesopores to macropores (100 to 1000 ms) and macropores ($T_2$ values above 1000 ms). We used these transition regions to facilitate a well-defined classification of pore sizes for the carbonate rocks because of their complex heterogeneous nature.

Figure 4 presents the pore size distributions of the six Indiana limestone samples. Notice that the curves for the six samples have very similar shapes, with the distribution of pore sizes and average relaxation times being essentially the same regardless of the selected sample. The plots themselves show bimodal distributions with $T_2$values varying between 0.1 ms and about 9000 ms. The bimodality $T_2$ distributions suggest that the samples are composed of both micro/mesopores (on average 31% of the pore volume) and macropores (about 69%). The bimodality also indicates the presence of a discontinuous range of pore sizes reflecting considerable heterogeneity of the samples.

Figure 5 shows the distributions of $T_2$ times of the four coquina samples. Samples MC15P1_B and MC15P2 exhibited bimodal curves reflecting the internal pore heterogeneity present in these samples. The curves for samples MC20P1 and MC20P2, on the other hand, are very much unimodal, thus highlighting the far more homogeneous pore size distributions of these two samples. There is a predominance of macropores (about 77% of the pores are in the macropores range), for microprosity and mesoporosity this value is 23% on average for all samples. It is also observed that the contribution of smaller pores concerning total porosity is not significant.

Figure 6 shows the pore size distributions for the three silurian dolomite samples analyzed. As observed for the Indiana limestone samples, the curves for the three silurian dolomite samples show similarity between them, showing that, regardless of the selected sample, it will represent well the other two samples analyzed. $T_2$ values range from 0.1 ms to 9000 ms in a unimodal distribution. The high occurrence of pore size above 100 ms (average of 79%) suggests that the sample is formed mainly by macropores.

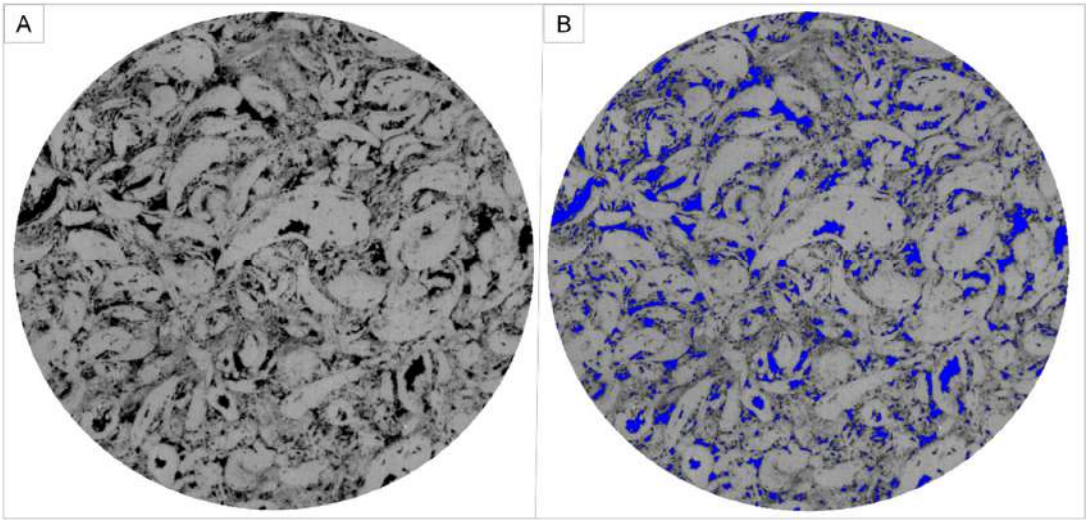


**Fig. 3.** MicroCT slices of sample MC20P2 with a voxel size of 25: (A) Grayscale image with pores in black and the rock matrix in gray; (B) Grayscale image with the segmented pores in blue.

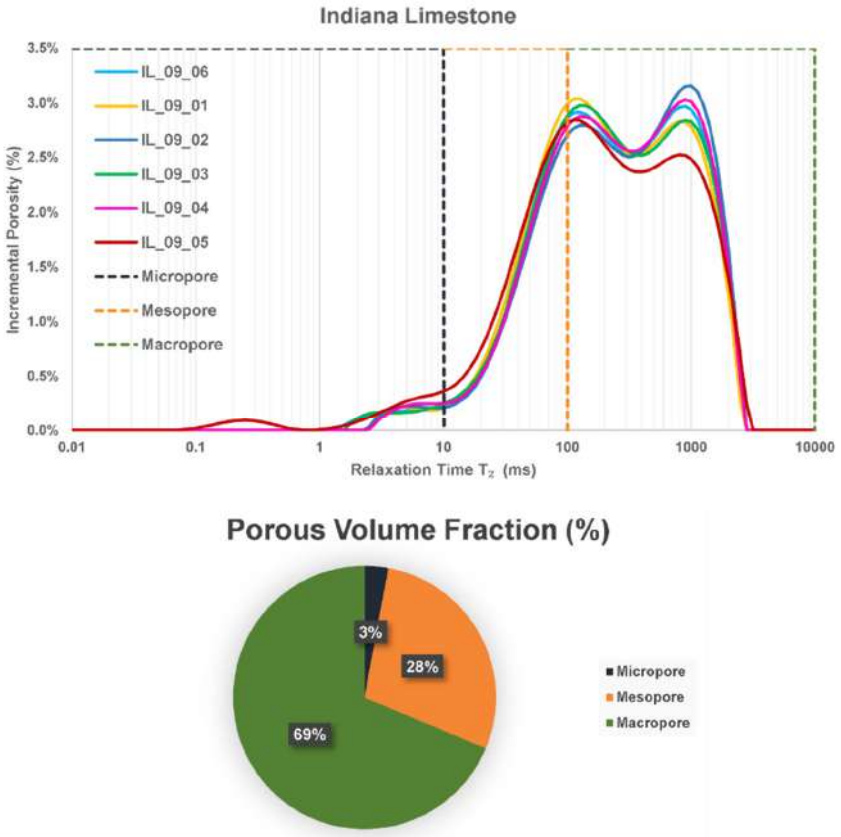


**Fig. 4.** Distribution of $T_2$ times for Indiana limestone samples (top) and volumetric fractions of the pore space partitioning (micropore, mesopore and macropore).

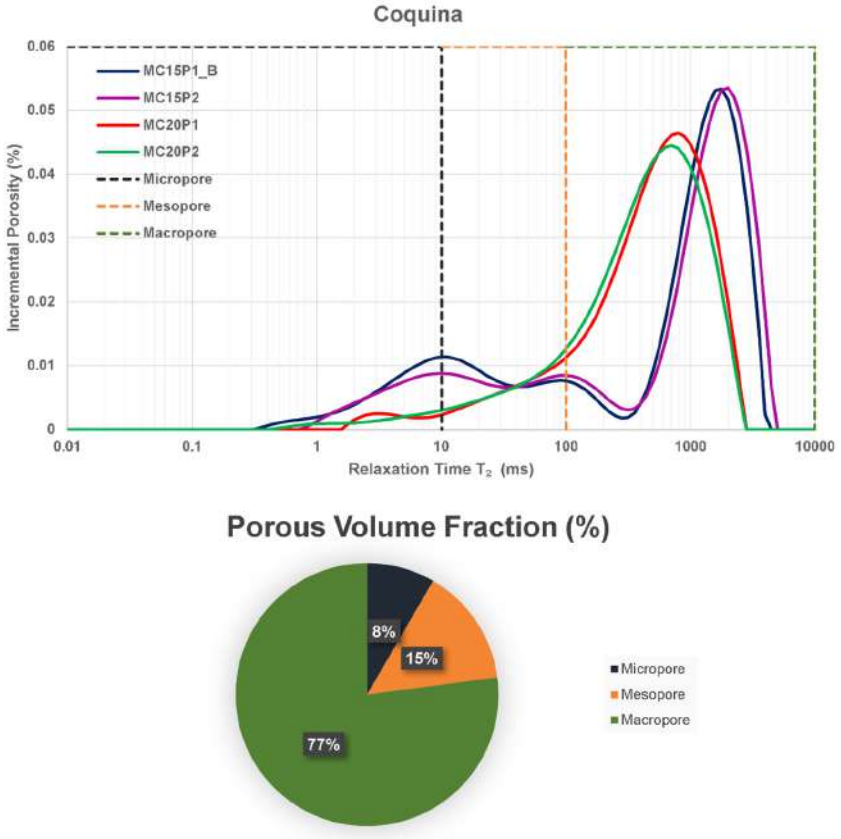


**Fig. 5.** Distribution of $T_2$ times for coquina samples and volumetric fractions of pore space partitioning (micropore, mesopore and macropore).

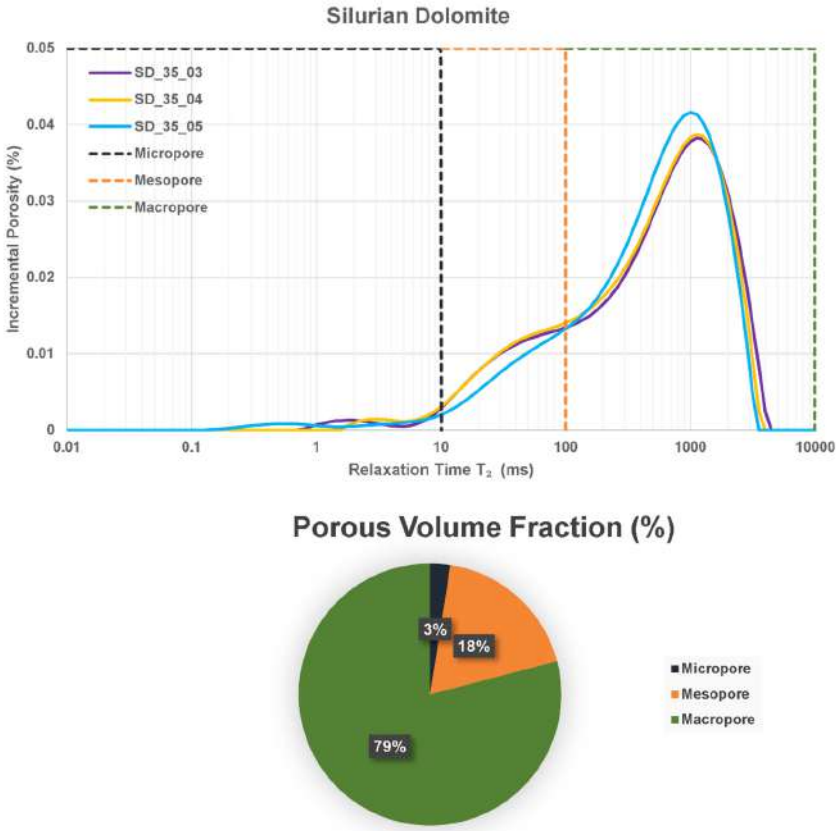


**Fig. 6.** Distribution of $T_2$ times for silurian dolomite samples and volumetric fractions of pore space partitioning (micropore, mesopore, and macropore).

Kazemi et al. (2020) previously listed $S_{gt}$ values for limestones having porosity values of 15% (similar porosities as our samples as shown in Fig. 1). Their $S_{gt}$ values ranged from 40% to about 60%, consistent with our silurian dolomite and coquina results, except for coquina sample MC15P1_B. When analyzing the $T_2$ time distributions of the Indiana limestone samples, in comparison with the other samples, we noted that this group had the highest percentage of microporosity. According to Suzanne and Billiote (2004), among others, high levels of microporosity diminishes gas trapping due to the low proportion of pore body and pore throats. This is also consistent with MC15P1_B coquina sample having an $S_{gt}$ value of 36%, not too much different from those of the Indiana limestones. The proportion of micro- and meso-porosity porosity for this sample was 31%, while the average of the coquina samples was only 23% (the same as for the Indiana limestone samples). Micro/mesoporosities greater than 30% hence seemed to have negative influence on gas trapping.

A useful complementary analysis to NMR is the characterization of the distribution of pore openings (e.g., their radii) using MICP. With this approach, the entire pore system represented by pore bodies (corresponding to the largest voids) and pore throats (connections between pore bodies) can be evaluated (Yuan and Rezaee, 2019). Figure 7 shows the pore throat size distributions, obtained via MICP tests, for the analyzed samples, as well as the volumetric fraction of pores partitioned into micro-, meso- and macroporosity. As noted earlier reported, only three samples were submitted to MICP tests based on the choice of $S_{gt}$ values (high, medium, and low value), i.e., samples SD_35_03 (silurian dolomite), MC20P2 (coquina), and IL_09_05 (Indiana limestone). The throat size partitioning scheme described by Gyllensten et al. (2008) was used to differentiate between different regions of the pore system: micropores from 0 to 0.5 µm, mesopores from 0.5 to 5 µm, and macropores above 5 µm.

The pore throat size distribution graph for the Indiana limestone sample in Fig. 7 shows a high percentage of throats in the micro/mesopore scale, about 60%, indicating that this sample is mostly composed of pores connected to small throats. The other two samples had similar profiles, indicating that the coquina and silurian dolomite samples contain mostly pores connected to large throats, with the volumetric fractions in the macroporosity scale being 88% and 77%, respectively.

The combined use of NMR and MICP results enables a conversion of the relaxation time distributions into pore radii distributions by superimposing the NMR curve over the MICP curve, and equating the peaks of the curves. Once it is verified that the distributions are well correlated, the surface relaxivity $\rho_2$ in Eq. (1) can be adjusted until the distributions present the same maximum as seen in Fig. 8 (Lima, et al., 2020). This correlation of the results makes it possible to partition the pores (e.g., Gyllensten et al., 2008).

Correlations of the NMR and MICP curves for samples SD_35_03 (silurian dolomite), MC20P2 (coquina) and IL_09_05 (Indiana limestone) are presented in Fig. 8. The Silurian Dolomite sample shows a reasonable correlation between the two curves, with the sample containing mostly macropores (about 77% of the pores), connected to large throats. The percentage of micropores and mesopores is only 23%, indicating that microporosity does not significant contribute to total porosity. The Coquina sample similarly shows a good close overlapping of the NMR and MICP curves. The sample is formed mainly by macropores (about 69% of the pores) connected to large throats, while the percentage of micro- and mesopores being 31%.

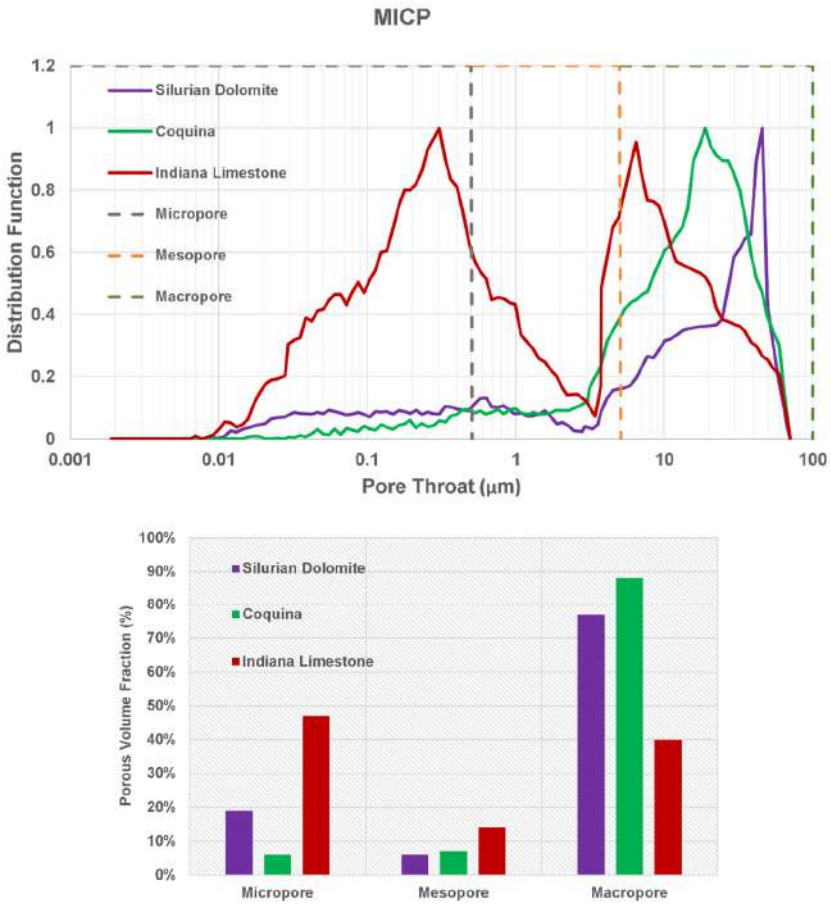


**Fig. 7.** Pore throat size distributions of the silurian dolomite, coquina, and Indiana limestone samples and volumetric fractions of the pore space partitions (micropore, mesopore and macropore) for each group of samples.

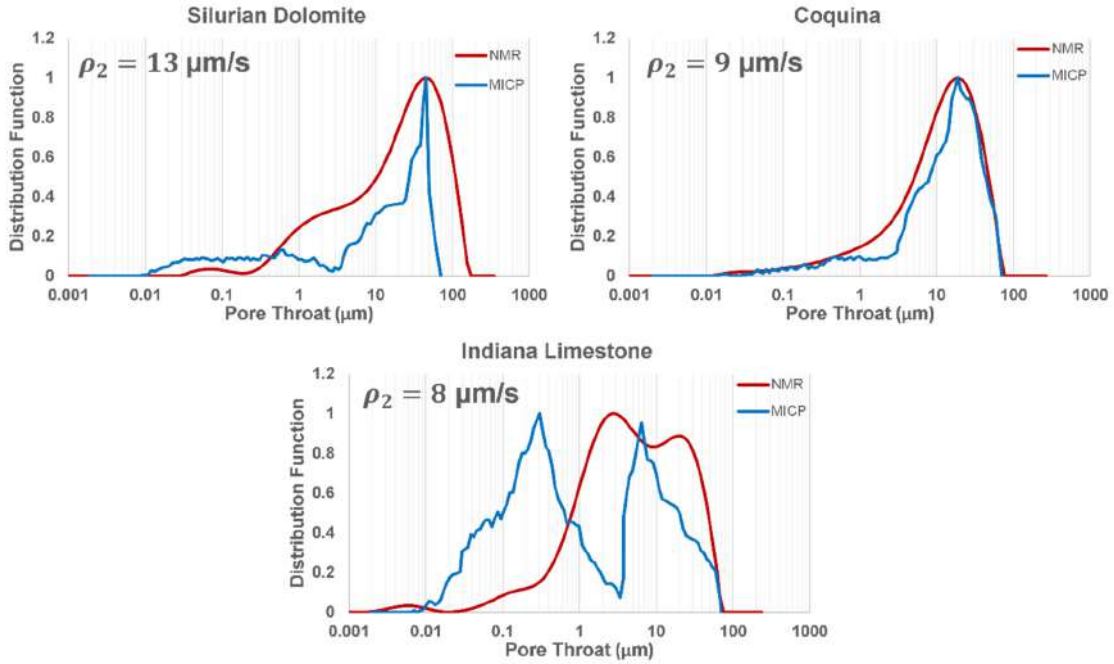


**Fig. 8.** Correlation between the NMR and MICP results for silurian dolomite sample SD_35_03, coquina sample MC20P2 and Indiana limestone sample IL_09_05.

By comparison, Indiana limestone sample IL_09_05 shows a relatively poor correlation in Fig. 8 between the NMR and MICP curves. Still, both curves indicate a bimodal pore distribution, with pore throats in mostly the micropore and mesopore regions. The MICP analysis indicates that about 54% of the pore throats are in the micropore and mesopores regions (following the scheme of Gyllenstein et al., 2008). With this analysis, we corroborate the view that Indiana limestone sample (IL_09_05) is formed mainly by small pores connected to small throats, unlike the two other samples. Fig. 8 also presents important information about the relaxivity $\rho_2$. The values used here (8, 9 and 13 μm/s) are typical of carbonate rocks.

The results obtained using NMR and MICP showed that the Indiana limestone samples have a high percentage of micropores and mesopores in their structure and that these pores are connected to throats also at the micropore and mesopores scale. Thus, we conclude that the microporosity and mesoporosity in these samples are the main cause of the low $S_{gt}$ values, conforming that gas trapping decreases substantially with an increase in relatively small pores. According to Jerauld (1997), gas trapping in micropores is not effective and will occur only at relatively high initial or maximum gas saturations. Changes in the saturation of trapped gas with increasing maximum gas saturation decreases with increasing maximum gas saturation, eventually approaching zero, thus indicating little entrapment in microporosity.

The silurian dolomite and coquina samples did not show significant proportions of micropores in their structures in terms of changing the trapping capacity of these samples. To further investigate this, we investigated the pore structure of these samples using microCT, in addition to obtaining estimates of the pore size distribution (via NMR) and the pore throat size distribution (via MICP). The skeletons generated for each sample made it possible to extract information about the pore connectivity (Godoy et al., 2019; Sahimi et al., 2012). The coordination number (or pore connectivity) represents the number of pore bodies that are connected with adjacent pores. Fig. 9 presents a comparison of coordination number versus frequency of the silurian dolomite SD_35_03 and coquina MC20P2 samples. The silurian dolomite sample showed better connectivity than the coquina sample. The coquina sample, in turn, had a higher frequency of pores connected (up to 7 throats). These results are opposite to those observed by Jerauld (1997), likely because the silurian dolomite sample with its better connectivity than the coquina sample, generated greater gas trapping.

For better characterization of the connectivity, a pore frequency graph by connection number was generated for different pore radii (Fig. 10). For pores with smaller radii we observed that coquina presents a higher frequency for all coordination numbers. Once the pore radius increases, the frequency became higher for the silurian dolomite sample regardless of coordination number. Making a parallel with the $S_{gt}$ values, we observed that profile of samples that trapped more gas are the samples that have pores with larger radii and better connectiveness. According to Blunt et al. (2013), the water films increase in the throats and along the pore walls as the water pressure increases during imbibition of water-wettable rocks. This increase occurs until the non-wetting fluid (gas in our case) loses contact with the surface of the solid. In this situation, all engulfed throats can become filled by wetting fluid while the the non-wetting phase is retained in the pore bodies, leading to a considerable amount of trapping in those pores since they contain most of the void volume in a rock (Fleury and Romero-Samiento, 2016; Krevor et al., 2015). Even with the silurian dolomite samples having pores better connected than the coquina samples (which would make gas trapping difficult), the frequency of larger pores in its structure was decisive to favor more gas trapping as compared to the coquina samples.

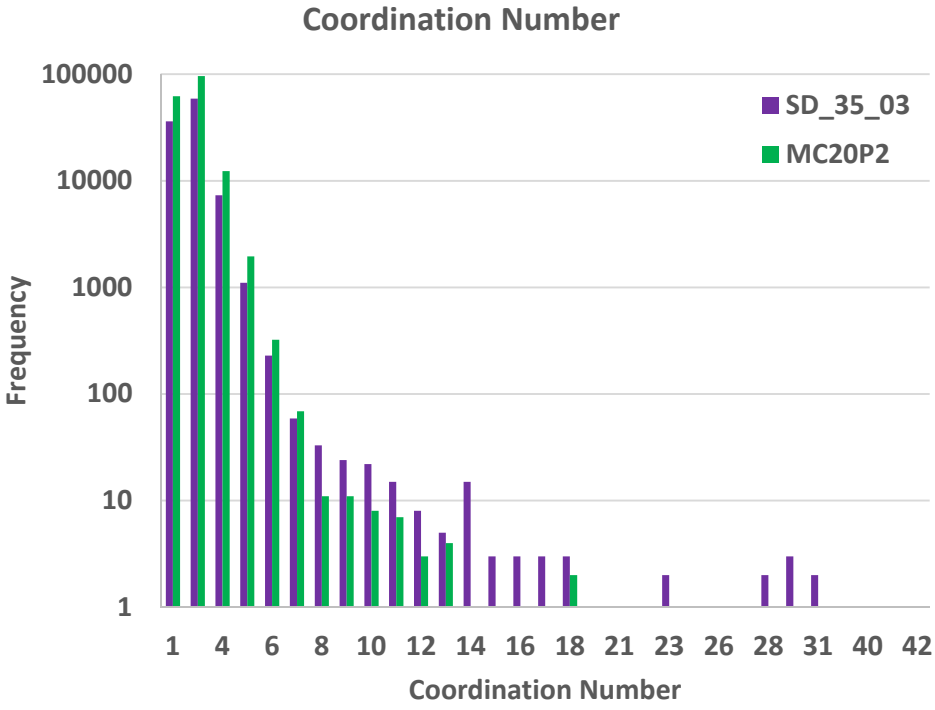


**Fig. 9.** Comparison of coordination numbers by frequency of silurian dolomite samples SD_35_03 (in purple) and of coquina sample MC20P2) (in green).

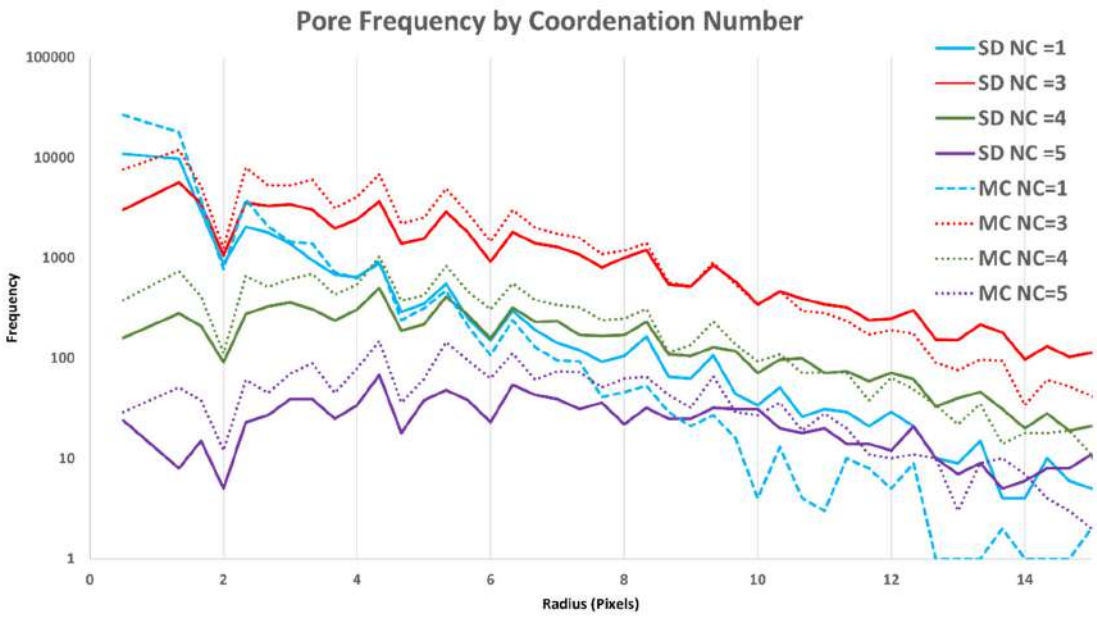


**Fig. 10.** Pore frequency by coordination number for different pore sizes for the silurian dolomite (SD) and coquina (MC) samples.

## CONCLUSIONS

Our research focused on the effects of pore structure, pore size distribution and pore connectivity on observed values of $S_{gt}$ in carbonate rock samples having very similar porosity values. NMR and MICP studies were performed on silurian dolomite, coquina, and Indiana limestone samples. Integration of the NMR and MICP methods enabled the estimates of the surface relaxation necessary to transform relaxation times into the pore size distribution, which in turn enabled the partitioning of pores into micro-, meso-, and macropores. MicroCT images were further used to obtain skeletons that provided the necessary input data (points, segments, and nodes) to generate 3D pore spaces and their connections.

The analysis of the pore bodies and pore throats through NMR and MICP could explain some of the observed variations in measured $S_{gt}$ values. For the Indiana limestone samples a considerable volume of pores existed within the micropore and mesopore ranges. Since microporosity interferes with effective gas trapping, this caused lower $S_{gt}$ values of these samples compared to the coquina and Indiana limestone plugs with less micropores and mesopores in their pore structure.

The 3D characterization of the pore space using microCT images provided an attractive means of explaining the high $S_{gt}$ values obtained for the silurian dolomite and coquina samples. We observed that even with a well-connected pore network, the frequency of pores with larger radii was decisive for greater trapping of the silurian dolomite sample compared to the coquina sample, thus showing that pore radii exert a greater influence on gas trapping than pore connectivity.

*Acknowledgements.* This research was carried out in association with ongoing R&D projects registered as ANP 19027-2, "Desenvolvimento de infraestrutura para pesquisa e desenvolvimento em recuperação avançada de óleo – EOR no Brasil" (UFRJ/Shell Brasil/ ANP) setting-up a advanced EOR Lab facility for R&D in Brasil, and ANP 20163-2, "Análise experimental da recuperação de petróleo para as rochas carbonáticas do pré-sal brasileiro através da injeção alternada de $CO_2$ e água", sponsored by Shell Brasil under the ANP R&D levy as "Compromisso de Investimentos com Pesquisa e Desenvolvimento". This study was financed in part by the Coordenação de Aperfeiçoamento de Pessoal de Nível Superior- Brasil (CAPES) - Finance Code 001 and carried out with the support of CNPq (National Council of Scientific and Technological Development, Brazil). We also thank the research teams of LRAP/COPPE/UFRJ.

## REFERENCES

Afzali, S., Rezaei, N., Zendehboudi, S., 2018. A comprehensive review on enhanced oil recovery by water alternating gas (WAG) injection. Fuel, 227, 218–246. https://doi.org/10.1016/j.fuel.2018.04.015

Aissaoui, A., 1983. Etude théorique et expérimentale de l'hystérésis des pressions capillaires et des perméabilités relatives en vue du stockage souterrain de gaz. Ecole des Mines de Paris, Paris.

Alyafei, N., 2015. Capillary trapping and oil recovery in altered-wettability carbonate rock. PhD thesis. Dept. of Earth Science and Engineering, Imperial College London.

Blunt, M., Bijeljic, B., Dong, H., Gharbi, O., Iglauer, S., Mostaghimi, P., Pentland, C., 2013. Pore-scale imaging and modelling. Adv. Water Resour., 51, 197–216. DOI: https://doi.org/10.1016/j.advwatres.2012.03.003

Bona, N., Garofoli, L., Radaelli, F., 2014. Trapped gas saturation measurements: New perpectives. SPE Annual Technical Conference and Exhibition, Amsterdam, The Netherlands, SPE- 170765-MS. https://doi.org/10.2118/170765-MS

Element, D., Master, J., Sargent, N., Jayasekera, A., Goodyear, S., 2003. Assesment of three-phase relative permeability models using laboratory hysteresis data. SPE Int. Improved Oil Recovery Conf. in Asia Pacific, Kuala Lumpur, Malaysia, SPE-84903-MS. https://doi.org/10.2118/84903-MS

Fatemi, S.M., Sohrabi, M., 2013. Experimental and theoretical investigation of oil and gas trapping under two- and three-phase flow including water alternating gas (WAG) injection. SPE Annual Techn. Conf. and Exhibition, New Orleans, Louisiana, USA, SPE-166193-MS. https://doi.org/10.2118/166193-MS

Faybishenko, B.A., 1995. Hydraulic behavior of quasi-saturated soils in the presence of entrapped air: Laboratory experiments. Water Resour. Res., 31, 2421–2435. https://doi.org/10.1029/95WR01654

Fayer, M.J., Hillel, D., 1986. Air encapsulation: II. Profile water storage and shallow water table fluctuations. Soil Sci. Soc. Am. J., 50, 572–577. https://doi.org/10.2136/sssaj1986.03615995005000030006x

Fleury, M., Romero-Sarmiento, M.. 2016. Characterization of shales using T1–T2 NMR maps. J. Petrol. Sci. Eng., 137, 55–62. https://doi.org/10.1016/j.petrol.2015.11.006

Ge, X., Myers, M.T., Liu, J., Fan, Y., Zaid, M.A., Zhao, J., Hathon, L., 2021. Determining the transverse surfave relaxivity of reservoir rocks: A critical review and perspective. Marine and Pet. Geol., 126. https://doi.org/10.1016/j.marpetgeo.2021.104934

Godoy, W., Pontedeiro, E.M., Hoerlle, F., Raoof, A., van Genuchten, M.Th., Santiago, J., Couto, P., 2019. Computational and experimental pore-scale studies of a carbonate rock sample. J. Hydrol. Hydromech., 67, 4, 372–383. http://dx.doi.org/10.2478/johh-2019-0009

Gonçalves, R.D., Teramoto, E.H., Engelbrecht, B.Z, Soto, M.A., Chang, H.K van Genuchten, M.Th., 2019. Quasi-saturated layer: Implications for estimating recharge and groundwater modeling. Groundwater, 58, 3, 432–440. https://doi.org/10.1111/gwat.12916

Gyllensten, A., Al-Hammadi, M. I., Abousrafa, E., Boyd, A., Ramamoorthy, R., Neumann, S., Neville, T.J., 2008. A new workflow for comprehensive petrophysical characterization of carbonate reservoirs drilled with water-base muds. Abu Dhabi Int. Petrol. Exhibition and Conf., Abu Dhabi, UAE, SPE-118380-MS. https://doi.org/10.2118/118380-MS

Hamon, G., Suzanne, K., Billiote, J., Trocme, V., 2001. Field-wide variations of trapped gas saturation in heterogeneous sandstone. SPE Annual Techn. Conf. and Exhibition, New Orleans, Louisiana, SPE-71524-MS. https://doi.org/10.2118/71524-MS

Herlinger, R.J., Zambonatto, E.E., de Ros, L.F., 2017. Infuence of diagenesis on the quality of lower Cretaceous Pre-Salt Lacustrine carbonate reservoirs from Northern Campos Basin, offshore Brazil. J. Sedim. Res., 87, 12, 1285–1313. https://doi.org/10.2110/jsr.2017.70

Jerauld, G.R., 1997. Prudhoe Bay gas/oil relative permeability. SPE Res. Eng., 12, SPE-35718-PA, 66–73. https://doi.org/10.2118/35718-PA

Kazemi, F., Azin, R., Osfouri, S., 2020. Evaluation of phase trapping models in gas-condensate systems in an unconsolidated sand pack. J. Petrol. Sci. Eng., 195, 107848. https://doi.org/10.1016/j.petrol.2020.107848

Khisamov, R.S., Bazarevskaya, V.G., Burkhanova, I.O., Kuzmin, V.A., Bolshakov, M.N., Marutyan, O.O.. 2020. Influence of the pore space structure and wettability on residual gas saturation. Georesour., 22, 2, 2–7. DOI:10.18599/grs.2020.2.2-7

Krevor, S., Blunt, M.J., Benson, S.M., Pentland, C.H., Reynolds, C., Al-Menhali, A., Niu, B., 2015. Capillary trapping for geologic carbon dioxide storage – From pore scale physics to field scale implications. Int. J. Greenh. Gas Control, 40, 221–237. https://doi.org/10.1016/j.ijggc.2015.04.006

Lai, J., Wang, G., Wang, Z., Chen, J., Pang, X., Wang, S., Fan, X., 2018. A review on pore structure characterization in tight sandstones. Earth Sci. Rev., 117, 436–457. https://doi.org/10.1016/j.earscirev.2017.12.003

Li, W., Lu, S., Xue, H., Zhang, P., Hu, Y., 2016. Microscopic pore structure in shale reservoir in the argillaceous dolomite from the Jianghan Basin. Fuel, 181, 1041–1049. https://doi.org/10.1016/j.fuel.2016.04.140

Lima, M.C., Pontedeiro, E.M., Ramirez, M.G., Favoreto, J., Santos, H.N., van Genuchten, M.Th., Raoof, A., 2022. Impacts of mineralogy on petrophysical properties. Transp. Porous Media, 145, 103–125. https://doi.org/10.1007/s11242-022-01829-w

Lima, M.C., Pontedeiro, E.M., Ramirez, M., Boyd, A., van Genuchten, M.Th., Borghi, L., Raoof, A., 2020. Petrophysical correlations for the permeability of coquinas (carbonate rocks). Transp. Porous Media, 135, 287–308. https://doi.org/10.1007/s11242-020-01474-1

Meiboom, S., Gill, D., 1958. Modified spin-echo method for measuring nuclear relaxation times. Rev. Sci. Instrum., 29, 688. https://doi.org/10.1063/1.1716296

Mohammadian, S., Geistlinger, H., Vogel, H.-J., 2015. Quantification of gas-phase trapping within the capillary fringe using computed microtomography. Vadose Zone J., 14, 1–9. https://doi.org/10.2136/vzj2014.06.0063

Ni, H., Boon, M., Garing, C., Benson, S.M., 2019. Prediction CO2 resudual trapping ability based on experimental petrophysical properties for different sandstone types. Int. J. Greenh. Gas Control, 86, 158–176. https://doi.org/10.1016/j.ijggc.2019.04.024

Otsuki, B., Takemoto, M., Fujibayashi, S., Neo, M., Kokubo, T., Nakamura, T., 2006. Pore throat size and connectivity determine bone and tissue ingrowth into porous implants: Three-dimensional micro-CT based structural analyses of porous bioactive titanium implants. Biomaterials, 27, 892–900. DOI: 10.1016/j.biomaterials.2006.08.013

Raeini, A.Q., Bijeljic, B., Blunt, M.J., 2015. Modelling capillary trapping using finite volume simulation of two-phase flow directly on micro-CT images. Adv. Water Resour., 83, 102–110. https://doi.org/10.1016/j.advwatres.2015.05.008

Raoof, A., Nick, H.M., Hassanizadeh, S.M., Spiers, C.J., 2013. Poreflow: A complex pore-network model for simulation of reactive transport in variably saturated porous media. Comp. Geosci., 61, 160–174. https://doi.org/10.1016/j.cageo.2013.08.005

Ruspini, L.C., Farokhpoor, R., Oren, P.E., 2017. Pore-scale modeling of capillary trapping in water-wet porous media: A new cooperative pore-body filling model. Adv. Water Resour., 108, 1–14. https://doi.org/10.1016/j.advwatres.2017.07.008

Sahimi, M., 2012. Flow and Transport in Porous Media and Fractured Rock: From Classical Methods to Modern Approaches. Wiley, Germany. DOI: 10.1002/9783527636693

Shao, X., Pang, X., Li, L., Zheng, D., 2017. Fractal analysis of pore network in tight gas sandstones using NMR method: A case study from the Ordos Basin, China. Energy Fuels, 31, 10, 10358–10368. https://doi.org/10.1021/acs.energyfuels.7b01007

Silva, P.N., Gonçalvez, E.C., Rios, E.H., Muhammad, A., Moss, A., Pritchard, T., Azeredo, R.B., 2015. Automatic classification of carbonate rocks permeability from $^{1}$H NMR relaxation data. Expert Systems Appl., 9, 9, 4299–4309. https://doi.org/10.1016/j.eswa.2015.01.034

Silveira, T.M., Hoerlle, F., Rocha, A.S., Lima, M.C., Ramirez, M.G., Pontedeiro, E.M., van Genuchten, M.Th., Couto, P., 2022. Effects of carbonated water injection on the pore system of a carbonate rock (coquina). J. Hydrol. Hydromech., 70, 2, 257–268. DOI: https://doi.org/10.2478/johh-2022-0001

Souza, A.A., 2012. Estudo de Propriedades Petrofísicas de Rochas Sedimentares por Ressonância Magnética. PhD thesis, Materials Science and Engineering, São Paulo University, 207p.

Sun, H., Vega, S., Tao, G., 2017. Analysis of heterogeneity and permeability anisotropy in carbonate rock samples using digital rock physics. J. Petr. Sci. Eng., 156, 419–429.

https://doi.org/10.1016/j.petrol.2017.06.002

Suzanne, K., Billiote, J., 2004. Influence de la microporosité sur le piégeage du gaz dans un milieu poreaux naturel. Comptes Rendus Geosci., 336, 12, 1071–1078. https://doi.org/10.1016/j.crte.2004.04.010

Suzanne, K., Hamon, G., Billiotte, J., Trocme, V., 2003. Experimental relationships between residual gas saturation and initial gas saturation in heterogeneous sandstone reservoirs. SPE Annual Techn. Conf. and Exhibition, Denver, Colorado, SPE-84038-MS. https://doi.org/10.2118/84038-MS

Tanino, Y., Blunt, M., 2013. Laboratory investigation of capillary trapping under mixed-wet conditions. Water Resour. Res., 49, 7, 4311–4319. https://doi.org/10.1002/wrcr.20344

Tanino, Y., Blunt, M., 2012. Capillary trapping in sandstone and carbonates: Dependence on pore structure. Water Resour. Res., 48, 8525. DOI: 10.1029/2011WR011712

Trevizan, W., Netto, P., Coutinho, B., Machado, V.F., Rios, E.H., Chen, S., Romero, P., 2014. Method for predicting permeability of complex carbonate reservoirs using NMR logging measurements. Petrophys., 55, 03, SPWLA-2014-v55n3a4, 240–252.

Washburn, E.W., 1921. Note on a method of determining the distribution of pore sizes in a porous material. Proc. Nat. Acad. Sci. USA, 7, 115–116. DOI: 10.1073/pnas.7.4.115

Wang, S., Tokunaga, T.K., Wan, J., Dong, W., Kim, Y,, 2016. Capillary pressure-saturation relations in quartz and carbonate sands: Limitations for correlating capillary and wettability influences on air, oil, and supercritical $CO_2$ trapping. Water Resour. Res., 52, 6671–6690. DOI: 10.1002/2016WR018816

Wildenschild, D., Sheppard, A.P., 2013. X-Ray imaging and analysis techniques for quantifying pore-scale structure and processes in subsurface porous medium systems. Adv. Water Resour., 51, 217–246. https://doi.org/10.1016/j.advwatres.2012.07.018

Yuan, Y., Rezaee, R., 2019. Comparative porosity and pore structure assessment in shales: Measurement techniques, infuencing factors and implications for reservoir characterization. Energies, 12, 2094. https://doi.org/10.3390/en12112094

Received 22 October 2022
Accepted 30 December 2022